ENHANCED FIRST APPROXIMATION FOR ICP-BASED GLOBAL MATCHING OF FREE-FORM CURVES IN SIDE-LOOKING RADAR GEOMETRY

D. I. Vassilaki [a], Ch. C. Ioannidis [a], A. A. Stamos [b]

[a] School of Rural and Surveying Engineering, [b] School of Civil Engineering
National Technical University of Athens, 9 Iroon Polytechniou Str, 15780 Zografos, Greece –
dimitra.vassilaki@gmail.com, cioannid@survey.ntua.gr, stamthan@central.ntua.gr

Commission III/1

KEY WORDS: Georeferencing, Matching, Feature, SAR, Radar, Adjustment

ABSTRACT:

The exploitation of linear features in aerial and satellite image orientation analysis has attracted much interest, due to the advantages of linear features, as opposed to salient points which are traditionally used in photogrammetric procedures. Linear features carry geometric information of higher quality, they can be extracted and matched more reliably, and they tend to be more stable during time. During the last decade, the Iterative Closest Point (ICP) algorithm has been introduced into various research projects, and, until recently, linear features were treated either as parametric curves, or as free-form/natural curves represented by cubic splines. Recent advances in the field show that ICP can handle linear features with an arbitrary mathematical representation, both for rigid and non-rigid transformations and for optical and SAR geometry. This paper presents an enhanced, more sophisticated single stage method for the computation of the first approximation which is one of the ICP requirements. The method is intended for ICP-based matching for the georeferencing of SAR images, using 3D linear features. The method uses the first order polynomial transformation, as an approximation to the arbitrary projection used in the SAR images. It exploits characteristic statistical properties of the curves in order to compute the polynomial coefficients. Various tests performed with the Single look Slant range Complex image (SSC) captured by TerraSAR-X in High Resolution SpotLight mode (HS), show the superiority of the proposed method as opposed to the two-stage similarity first approximation used in the past.

1.INTRODUCTION

The Iterative Closest Point (ICP) algorithm (Besl and McKay, 1992; Zhang, 1994), is a well-known and efficient tool for 3D point cloud registration. The ICP algorithm has also been used to coarsely align features between heterogeneous geospatial data (Butenuth *et al.*, 2007), to recover the exterior orientation of aerial images using parametric curves (Zalmanson, 2000), and, recently, to accomplish the bundle block adjustment problem using 3D natural cubic splines as Ground Control Features (GCFs) (Lee, 2008). Lee concluded that the use of linear features with an arbitrary mathematical representation should be investigated in future. During the same period an ICP-based method was introduced for the accurate 2D global matching of free-form linear features, using rigid transformation (Vassilaki *et al.*, 2008a). Linear features were treated as free-form curves of arbitrary geometry, which were represented as independent collections of consecutive nodes, joined with straight line segments, or with some other interpolation function.

Based on this method, Vassilaki *et al.*, (2009) performed accurate global matching in the case of projective geometry. 3D free-form linear features of the object space were matched with their 2D projection on optical and SAR images. Various projective transformations were used, such as polynomials, Direct Linear Transform (DLT) and Rational Polynomial Functions (RPFs). However, the method has inherited ICP's requirement for a good first approximation. The curves to be matched must be close enough to achieve convergence.

In (Vassilaki *et al.*, 2009) an automated pre-alignment (coarse registration) of the curves was performed, using the similarity transformation to bring the curves close to each other. The similarity transformation parameters were computed exploiting physical properties of the curves, in combination with exhaustive search techniques. The similarity transformation works well in the case of space-borne optical and SAR sensors, because the orbits' elevations are high enough and the image deformations due to terrain (and the distortions due to sensor for optical images) are comparatively small. Thus, the planar coordinates of a 3D feature can be considered as a good approximation of the 2D projected coordinates, after being scaled, translated and rotated appropriately.

In the case of unprocessed SAR images this in not always the result, since the geometric distortions due to the side-looking geometry and the nature of the SAR sensor are more severe. The similarity-based first approximation is sufficient when the projective transformation is the first order polynomial. For higher order projective transformations (DLT, RPFs), which are closer to the true geometry and the physical model of a SAR sensor, a better first approximation is needed. Vassilaki *et al.* (2009) used a two stage solution. Obviously a better approximation which leads to faster convergence without the need of two stage approximation is advantageous.

This paper presents an enhanced, more sophisticated single stage method for the computation of the first approximation. The method is intended for ICP-based matching for the georeferencing of SAR images, using 3D linear features. The method uses the first order polynomial transformation, to bring the curves to be matched, close enough for the ICP to converge. The coefficients of the polynomial transformation are computed exploiting characteristic statistical properties of the curves.

2.PROPOSED METHODOLOGY

In this paper, the proposed polynomial transformation for the automated pre-alignment of free-form curves is essentially an affine transformation (Equation 1). It is computed before performing accurate ICP-based matching, and it is better than the similarity transformation, as it can account for non-rigid distortions:

$$\begin{aligned} x &= aX + bY + c \\ y &= dX + eY + f \end{aligned} \tag{1}$$

where x, y are the 2D coordinates of the SAR image and X, Y are the horizontal object coordinates. If more than three homologous points were known, then it would be straightforward to compute the coefficients of the polynomial transformation using the Least Square Method (LSM). However, in the case of automated free-form curves matching, there is no prior knowledge of the correspondences of points. Instead, some characteristic properties which depend on the curve as a whole must be used. If the two curves represent the same physical feature (for example a road centerline), then a characteristic property of the SAR curve must be equal to the same characteristic property of the object curve:

$$\begin{aligned} P(x_1, y_{1,\dots}, x_n, y_n) = P(&aX_1 + bY_1 + c, dX_1 + eY_1 + f, \dots, \\ &aX_m + bY_m + c, dX_m + eY_m + f) \end{aligned} \tag{2}$$

The number of nodes n of the SAR curve is, in general, different from the number of nodes m of the object curve. In general, node x_i, y_i does not correspond to any of the nodes X_j, Y_j (and certainly $i \neq j$). At least six or more characteristic properties are needed to compute the 6 coefficients a, b, c, d, e, f of the polynomial transformation, in order to achieve robust results.

The statistical moments can be used as such characteristic properties of the curves. They have been used in many pattern recognition problems, since they transform the complicated geometry of an object to practically distinct numbers. Some moments are insensitive to scale and rotation (moment invariants with respect to projective transformation). In the present method these moments are not used, since the objective is to use the moments to compute the coefficients of the transformation, and not to eliminate it. Moment invariants could be used to identify features' correspondence between networks of free-form curves.

The physical interpretation of the moments used in this paper, is the average and standard deviation for the first and second moment, while the third and the fourth moments indicate the skewness and the kurtosis of the variable respectively (Abramowitz and Stegun, 1972; Press *et al*., 1992).

In theory, the moments could be used to compute the parameters of any kind of transformation, such as the DLT or even the physical model of the SAR sensor. In practice, however, this is not possible because the equations of moments lead to non-linear LSM, which requires initial values of the parameters. Unfortunately, no such initial values are available for transformations other than the similarity, or the one proposed in this paper.

2.1Moment Equations

The kth moment of a continuous random variable about a value c is defined as:

$$\mu'_k = \int_{-\infty}^{\infty} (x-c)^k f(x)\,dx \tag{3}$$

where $f(x)$ is the probability density function. The kth moment of a discrete random variable f_j is given in Equation (4):

$$\mu'_k = \frac{1}{m}\sum_{j=1}^{m} (f_j - c)^k \tag{4}$$

In this paper the first moments of x and y coordinates about zero are used, which coincide with the centroid of the curve. The moments of the curve on the SAR image are given:

$$\mu'_{x1} = \frac{1}{n}\sum_{i=1}^{n} x_i \quad , \quad \mu'_{y1} = \frac{1}{n}\sum_{i=1}^{n} y_i \tag{5}$$

These moments should be equal to the moments of the transformed coordinates of the object curve:

$$\begin{aligned} \mu'_{X1} &= \frac{1}{m}\sum_{j=1}^{m} (a X_j + b Y_j + c) \\ \mu'_{Y1} &= \frac{1}{m}\sum_{j=1}^{m} (d X_j + e Y_j + f) \end{aligned} \tag{6}$$

In order to avoid huge numbers which will degrade the numerical computations, the normalized central moments are used for the higher moments:

$$\mu_{xk} = \sqrt[k]{\frac{1}{n}\sum_{i=1}^{n} (x_i - \mu'_{x1})^k} \quad , \quad \mu_{yk} = \sqrt[k]{\frac{1}{n}\sum_{i=1}^{n} (y_i - \mu'_{y1})^k} \tag{7}$$

These moments should also be equal to the corresponding moments of the object curve:

$$\begin{aligned} \mu_{Xk} &= \sqrt[k]{\frac{1}{m}\sum_{j=1}^{m} (a X_j + b Y_j + c - \mu'_{X1})^k} \quad , \\ \mu_{Yk} &= \sqrt[k]{\frac{1}{m}\sum_{j=1}^{m} (d X_j + e Y_j + f - \mu'_{Y1})^k} \end{aligned} \tag{8}$$

Another reason for the normalization of the higher order moments is to express the moments in the same units (length units or meters). Thus, all the equations of moments have the same (implicit) weight when the LSM is applied; numerical experiments with no, or other, normalizations led to poor results.

2.2Length Equation

Each moment applied to x and y coordinates provides 2 equations. Thus, the first 3 moment (k=1,2,3) provide 6 equations which should be sufficient to estimate the 6 unknown coefficients of the polynomial transformation, but they give poor results in some cases. Taking 4 moments, or 8 equations, and applying the LSM leads to somewhat better results, but it still lacks an acceptable quality. This could be explained by the fact that the polynomial transformation and the equation of moments for the x coordinates, are completely independent of the y coordinates. However, the x and y coordinates are coupled as they together define a (free form) curve. This coupling should be reflected to the equations. One way to achieve this is to exploit the fact that the correspondent curves have the same length (global matching):

$$L(x_1, y_1, \dots, x_n, y_n) = L(aX_1+bY_1+c, dX_1+eY_1+f, \dots, aX_m+bY_m+c, dX_m+eY_m+f) \quad (9)$$

Equation (9) can be written as:

$$\sum_{i=2}^{n} [(x_i - x_{i-1})^2 + (y_i - y_{i-1})^2]^{1/2} =$$

$$\sum_{j=2}^{m} \{[(aX_j+bY_j+c) - (aX_{j-1}+bY_{j-1}+c)]^2 + [(dX_j+eY_j+f) - (dX_{j-1}+eY_{j-1}+f)]^2\}^{1/2} = \quad (10)$$

$$= \sum_{j=2}^{m} \{[a(X_j - X_{j-1}) + b(Y_j - Y_{j-1})]^2 + [d(X_j - X_{j-1}) + e(Y_j - Y_{j-1})]^2\}^{1/2} = \sum_{j=2}^{m} L_j$$

Results derived from various tests made for this research, proved that the equations of 3 moments combined with the equation of the lengths greatly enhance the results. If 4 moments are used the results are slightly better, but 5 or more moments give no noticeable improvements.

3.LEAST SQUARES ADJUSTMENT

As there are at least 7 non-linear equations for 6 unknowns, the system of equations must be solved using the non-linear LSM. This implies that the equations must be linearized and initial values for the unknown coefficients must be computed. The partial derivatives of Equations (6), (8) and (10) with respect to the unknown parameters are shown in the Appendix.

The matrix equation of the iterative non-linear LSM is $[A][dx] = [B]$, where $[A]$ is the design matrix which contains the partial derivatives of each equation with respect to each unknown parameter. $[dx]$ is the vector of the adjustment values of the unknown parameters. The vector $[dx]$ which is computed by the first iteration of LSM, is used to update the initial values of the unknown parameters $[X^o]$: $[X^1] = [X^o] + [dx]$. The procedure is repeated until convergence $([dx] \approx \cdot)$.

The initial values $[X^o]$ of the unknown parameters can be found indirectly using the similarity transformation:

$$\begin{aligned} x &= X_0 + \mu(X\cos\phi + Y\sin\phi) = (\mu\cos\phi)X + (\mu\sin\phi)Y + X_0 \\ y &= Y_0 + \mu(-X\sin\phi + Y\cos\phi) = (-\mu\sin\phi)X + (\mu\cos\phi)Y + Y_0 \end{aligned} \quad (11)$$

where $X_\circ, Y_\circ$ is the translation, μ is the scale and φ is the rotation angle. It must be noted that in this case the similarity transformation is not used as a first approximation to the ICP algorithm, but only to compute the initial values for the application of the non-linear LSM. Comparing the similarity and the polynomial transformations (Equations (1) and (11)), the following initial values can be found:

$$\begin{aligned} a &= \mu\cos\phi \quad , \quad b = \mu\sin\phi \quad , \quad c = X_0 \\ d &= -\mu\sin\phi \quad , \quad e = \mu\cos\phi \quad , \quad f = Y_0 \end{aligned} \quad (12)$$

The parameters $X_\circ, Y_0, \mu, \phi$ of the similarity transformation can be determined as described in Vassilaki *et al.* (2008c). Specifically, the translation X_0, Y_0 is computed as the distance of the centroids of SAR curve (B) and the object curve (A):

$$X_0 = x_B - x_A \quad , \quad Y_0 = y_B - y_A \quad (13)$$

where $x_A = \dfrac{\int_{S_A} x(s)\,ds}{\int_{S_A} ds}$, $y_A = \dfrac{\int_{S_A} y(s)\,ds}{\int_{S_A} ds}$

$x_B = \dfrac{\int_{S_B} x(s)\,ds}{\int_{S_B} ds}$, $y_B = \dfrac{\int_{S_B} y(s)\,ds}{\int_{S_B} ds}$

The scale μ is computed as the ratio of the length of the two curves:

$$\mu = \frac{S_B}{S_A} \quad , \text{ where } \quad S_A = \int_{S_A} ds \ , \ S_B = \int_{S_B} ds \quad (14)$$

The rotation φ between the two curves is computed by trying all the possible rotation angles between 0^g and 400^g in small steps (for example 3^g). For each angle step the error is computed employing the ICP algorithm (as described later) to find homologous points. The rotation angle with the least error is chosen.

4.ICP BASED MATCHING FOR FREE-FORM CURVES

The method used in this paper matches free-form curves using the ICP algorithm as summarized below:

1. Compute the polynomial first approximation using moments and length equations.
2. Using the polynomial first approximation, project the 3D nodes of the object curve, remembering which 3D node is projected to each of the 2D nodes. The projection is sufficiently near to the SAR curve.
3. For each 2D node of the projected object curve, find its closest point in the SAR curve, thus producing homologous 3D object curve nodes and (2D) SAR curve points.
4. Using the homologous pairs compute the parameters of the arbitrary projection selected (DLT, rational function, etc), using the LSM.
5. Compute the error of the projection.
6. Using the computed parameters of the transformation make a new projection of the project curve, remembering which 3D nodes is projected to each of the 2D nodes.
7. Steps 3 to 6 are repeated until the error stabilizes.

From the above mentioned steps, the operation of step 3 needs further explanation. If the SAR curve were a straight line, its closest point to a node could be found analytically, by minimizing the function which gives the distance between the node and a point on the line. In reality though, the SAR curve is a free-form curve which is described by nodes linked with straight line segments, in the simplest case. This means that the analytical minimum may correspond to a point outside the line segment, and this may be true for all line segments. This leads to complexity and computational cost. If the nodes are linked with higher order curves (for example cubic splines) the analytical computation of the minimum will be iterative, which leads to more complexity, more computational cost and the need to ensure convergence.

To overcome the problems, it is proposed by the authors to split the SAR curve to a large number of consecutive interpolated points using the arbitrary type of curve that links the nodes (linear, cubic splines, etc). The closest point of the SAR curve to a node is found by computing the distance of all the points to the node, and choosing the one with the least

distance. Although this is computationally intensive, a closest point is sure to be found.

For this brute-force method to work the interpolation distance must be small, which leads to large computing power requirements. However these requirements are certainly within the capabilities of modern computers. It is also relatively easy to reduce the requirements using a divide and conquer technique described in (Vassilaki *et al.*, 2008b). Furthermore, the computational burden may be split to multiple cores, multiple processors, or even multiple computers in a standard LAN, using state of the art parallel techniques (e.g. Fortran 2008), as the computation of the closest point of each node is almost independent of one another ([Stamos *et al.*, 2009]).

5.APPLICATIONS

Two real world examples were used in order to test the proposed method. A high resolution TerraSAR-X image, captured in February 2009, was used. The 3D object space data were derived from an old medium scale topographic map (1:5000), which was compiled in the 1970s with photogrammetric stereo-restitution. The TerraSAR-X image is a High Resolution SpotLight (HS) image with single polarization (HH); it is a Single look Slant range Complex image (SSC).

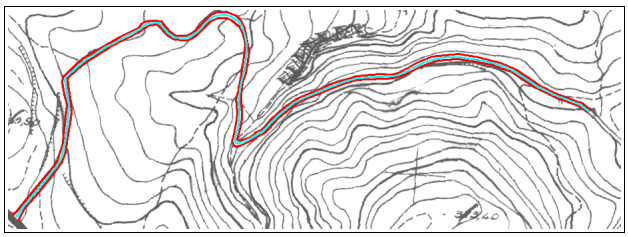

Figure 1. Example 2: Map road centerline (in cyan).

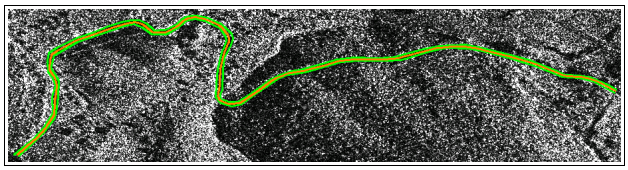

Figure 2. Example 2: SAR road centerline (in orange).

For each of the two examples, a free-form curve (common to the 2 data sets) was selected as a 3D linear feature. The curves of both examples represent road centerlines (Figures 1 and 2). The area of the examples is on the north east side of Athens. It is mountainous, contains some rural regions (villages and small towns) and is generally covered by sparse vegetation. During the recent forty years it has been subject to considerable development; new roads, buildings, and infrastructure in general. The terrain of the area is steep and the average slope is about 50%.

The 3D object coordinates refer to the Hellenic Geodetic Reference System 87 (HGRS87). The 2D SAR image coordinates refer to pixels. Thus, they are completely different and they do not fit on the same figure. For illustration purposes, a thumbnail of the 3D centerline is shown in the same figure with its 2D projections.

The DLT projection transformation was used to project the object coordinates to the SAR image. DLT is a first order RPF with common denominators for x and y. It has 11 independent coefficients which were computed using the road centerlines:

$$x = \frac{(a_1X + a_2Y + a_3Z + a_4)}{(c_1X + c_2Y + c_3Z + 1)}$$
$$y = \frac{(b_1X + b_2Y + b_3Z + b_4)}{(c_1X + c_2Y + c_3Z + 1)} \quad (15)$$

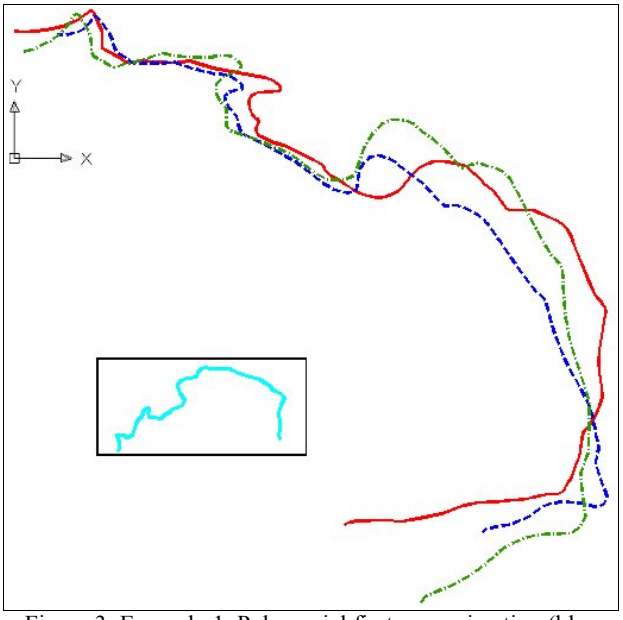

Figure 3. Example 1: Polynomial first approximation (blue dashed) using 4 moments.

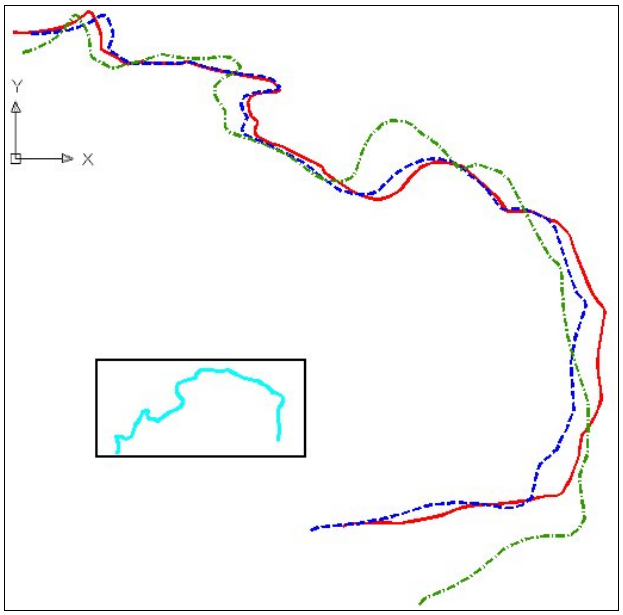

Figure 4. Example 1: Polynomial first approximation (blue dashed) using 4 moments and length equation.

The first approximation of the projections was computed using 3-8 moment equations, with or without the length equation. A total of 12 cases were computed. The RMS error of the first approximation was computed by performing a single ICP step between the first approximation and the curve on the SAR image. Specifically, the 4 moment equations gave less error than the 3 moment equations, but the difference of the errors was small and could not be identified in the scale of the figures. The 5 (or more) moment equations, gave almost identical RMS errors. For instance, in the first example:

- the 3 moments and the length equations gave RMS=44 pixels

- the 4 moments and the length equations gave RMS=36 pixels
- the 5-8 moments and the length equations gave RMS no better than 33 pixels.

Thus, in the following figures the results of only two cases are shown; 4 moment equations, with, and without, the length equation.

Figures 3-6 show the 2D SAR image coordinates. The flight (azimuth) direction is the y-axis on the figures, while the range direction is the x-axis. The distortion due to the SAR sensor of the road centerline is evident, if the SAR centerline (red) is compared to the object coordinates in the thumbnail (cyan).

In the first example (Figures 3 and 4), it is clear that the rigid nature of the similarity transformation (green-dashed) prevents it from modeling the SAR geometry as well as the polynomial transformation (blue-dashed). This is more evident in Figure 4, where the length equation pushes the polynomial first approximation (blue-dashed) very close to the SAR centerline (red). In Figure 3, the 4 moment equations have brought the polynomial first approximation (blue-dashed) near to the SAR centerline (red), but they have altered its length. Thus, it is impossible for the first approximation to be close to the SAR centerline all over its whole length. The length equation remedies this side effect and brings the first approximation (blue-dashed) very close to the SAR centerline (red), as it is shown in Figure 4. For illustration purposes the convergence of the ICP-based matching with the present method, versus the two stage method (Vassilaki *et al.,* 2009), is shown in Figure 7. The convergence with the present method appears with blue color. The converge with the two stage method appears with red (1st stage) and green (2nd stage) color.

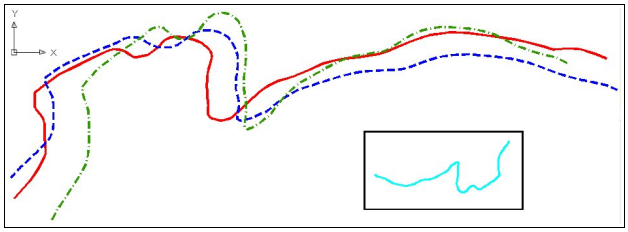

Figure 5. Example 2: Polynomial first approximation (blue dashed) using 4 moments.

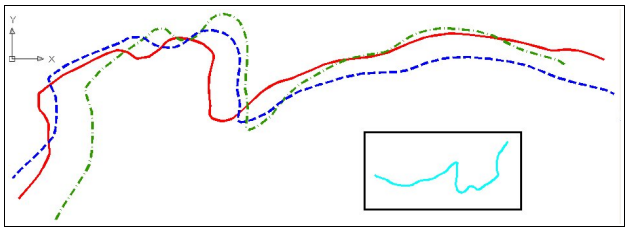

Figure 6. Example 2: Polynomial first approximation (blue dashed) using 4 moments and length equation.

In the second example (Figures 5 and 6), the polynomial first approximation (blue-dashed) is better than the similarity first approximation (green-dashed). This is also confirmed by the fact that ICP converges with the former but not with the latter approximation. In Figure 5, the 4 moment equations have brought the polynomial first approximation (blue-dashed) near to the SAR centerline (red), but they have not altered its length as in the first example. Consequently, as it is shown in Figure 6, the length equation has little effect in this example. Nevertheless, it is needed in some cases, and its small computational cost justifies its use in all cases.

Using the first approximation computed by 4 moments and length equations, the curves on the object space and the SAR image were matched. In Figures 8 and 9, the curve in the object space is cyan, the curve in the SAR image is red, the first approximation is blue-dashed, and the object space curve projected to the SAR image (matched curve) is black-dashed. The RMS error of the matched curves is 3.7m in the first example (Figure 8), and 1.4 m in the second example (Figure 9).

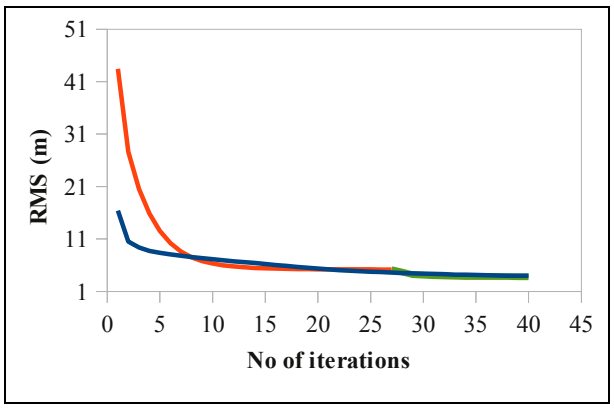

Figure 7. Convergence of the ICP-based matching with present method and the two stage method.

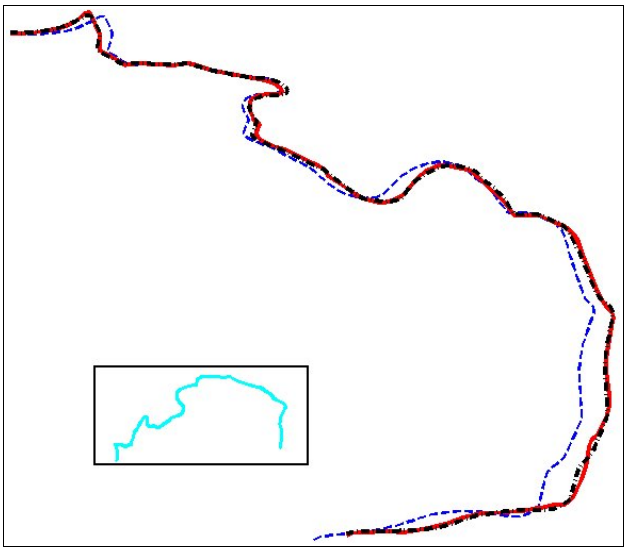

Figure 8. Example 1: Matched curves

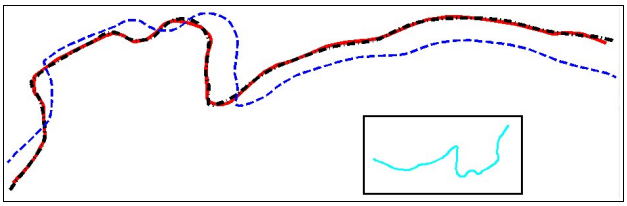

Figure 9. Example 2: Matched curves

6.CONSLUSIONS

A new method for obtaining the first approximation for ICP-based global matching of free-form curves in side-looking radar geometry was presented. The method uses the statistical moments and the length of the curves as characteristic properties. The characteristic properties depend on the whole of the curve and not on individual nodes. They can be used, as homologous entities, to compute the coefficients of the 1st order

polynomial transformation between the curves. The polynomial transformation brings the curves close enough, to trigger the convergence of the ICP algorithm in one stage. The method has been tested with real world examples and shows excellent results. For future research, the 2nd order polynomial transformation could be used as a first approximation.

REFERENCES

Abramowitz, M. and Stegun, I.A., 1972. Handbook of Mathematical Functions with Formulas, Graphs, and Mathematical Tables, 9th printing. New York: Dover, p. 928, 1972.

Besl, P.J. and McKay, N.D., 1992. A Method for Registration of 3-D Shapes. *IEEE Transactions on Pattern Analysis and Machine Intelligence,* 14(2), pp. 239-256.

Butenuth M, Gösseln G.v., Tiedge M, Heipke C., Lipeck U. and Sester M., 2007. Integration of heterogeneous geospatial data in a federated database. *ISPRS Journal of Photogrammetry & Remote Sensing,* 62(5), pp. 328–346.

Lee, W.H, 2008. Bundle block adjustment using 3D natural cubic splines. Ph.D. dissertation, The Ohio State University, U.S.A.

Press, W.H., Flannery, B.P., Teukolsky, S.A. and Vetterling, W.T., 1992. Moments of a Distribution: Mean, Variance, Skewness, and So Forth." §14.1 in Numerical Recipes in FORTRAN: The Art of Scientific Computing, 2nd ed. Cambridge, England: Cambridge University Press, pp.604-609.

Stamos, A.A., Vassilaki D.I. and Ioannidis, Ch.C., 2009. Speed Enhancement of Free-form Curve Matching with Parallel Fortran 2008. in B.H.V. Topping, P. Iványi, (Editors), *Proceedings of the First International Conference on Parallel, Distributed and Grid Computing for Engineering*, Civil-Comp Press, Stirlingshire, UK.

Vassilaki, D., Ioannidis, Ch. and Stamos, A., 2008a. Registration of 2D Free-Form Curves Extracted from High Resolution Imagery using Iterative Closest Point Algorithm. EARSeL's Workshop on Remote Sensing – New Challenges of High Resolution, March 5-7, Bochum, Germany, pp.141-152.

Vassilaki, D., Ioannidis, Ch., Stamos, A., 2008b. Computation of the Closest Points for Matching Curves of Different Dimensionality. 3rd International Conference: From Scientific Computing to Computational Engineering, July 9-12, Athens, Greece.

Vassilaki, D., Ioannidis, Ch. and Stamos, A., 2008c. Geospatial Data Integration using Automatic Global Matching of Free-Form Curves. *Digital Earth Summit on Geoinformatics: Tools for Global Change Research*, November 12-14, Potsdam, Germany, Wichmann Verlag, Heidelberg, pp. 195-200.

Vassilaki, D., Ioannidis, Ch. and Stamos, A., 2009. Registration of Unrectified Optical and SAR imagery over Mountainous Areas through Automatic Free-form Features Global Matching. *International Archives of Photogrammetry and Remote Sensing* (38), Part 1-4-7/W5 (on CD-ROM).

Zalmanson, H.G., 2000. Hierarchical Recovery of Exterior Orientation from Parametric and Natural 3-D Curves. *International Archives of Photogrammetry and Remote Sensing* (33), Part B3, pp. 610-617.

Zhang, Z., 1994. Iterative Point Matching for Registration of Free-form Curves and Surfaces. *International Journal of Computer Vision*, 13(2), pp. 119-152.

ACKNOWNLEDGMENTS

The authors are grateful to the School of Rural and Surveying Engineering for providing SAR data.

APPENDIX A. PARTIAL DERIVATIVES

$$\frac{\partial \mu_{X1}'}{\partial a}=\frac{1}{m}\sum_{i=1}^{m} X_j=\bar{X} \quad , \quad \frac{\partial \mu_{X1}'}{\partial b}=\frac{1}{m}\sum_{i=1}^{m} Y_j=\bar{Y}$$

$$\frac{\partial \mu_{X1}'}{\partial c}=\frac{1}{m}\sum_{i=1}^{m} 1=1$$

$$\frac{\partial \mu_{Y1}'}{\partial d}=\bar{X} \quad , \quad \frac{\partial \mu_{Y1}'}{\partial e}=\bar{Y} \quad , \quad \frac{\partial \mu_{Y1}'}{\partial f}=1$$

$$\frac{\partial \mu_{Xk}}{\partial a}=\frac{(\mu_{Xk})^{1-k}}{m}\cdot\sum_{j=1}^{m}(aX_j+bY_j+c-\mu_{X1}')^{k-1}(X_j-\bar{X})$$

$$\frac{\partial \mu_{Xk}}{\partial b}=\frac{(\mu_{Xk})^{1-k}}{m}\cdot\sum_{j=1}^{m}(aX_j+bY_j+c-\mu_{X1}')^{k-1}(Y_j-\bar{Y})$$

$$\frac{\partial \mu_{Xk}}{\partial c}=\frac{(\mu_{Xk})^{1-k}}{m}\cdot\sum_{j=1}^{m}(aX_j+bY_j+c-\mu_{X1}')^{k-1}(1-1)=0$$

$$\frac{\partial \mu_{Yk}}{\partial d}=\frac{(\mu_{Yk})^{1-k}}{m}\cdot\sum_{j=1}^{m}(dX_j+eY_j+f-\mu_{Y1}')^{k-1}(X_j-\bar{X})$$

$$\frac{\partial \mu_{Yk}}{\partial e}=\frac{(\mu_{Yk})^{1-k}}{m}\cdot\sum_{j=1}^{m}(dX_j+eY_j+f-\mu_{Y1}')^{k-1}(Y_j-\bar{Y})$$

$$\frac{\partial \mu_{Yk}}{\partial f}=\frac{(\mu_{Yk})^{1-k}}{m}\cdot\sum_{j=1}^{m}(dX_j+eY_j+f-\mu_{Y1}')^{k-1}(1-1)=0$$

$$\frac{\partial L}{\partial a}=\sum_{j=2}^{m}\frac{1}{L_j}\left[a(X_j-X_{j-1})+b(Y_j-Y_{j-1})\right](X_j-X_{j-1})$$

$$\frac{\partial L}{\partial b}=\sum_{j=2}^{m}\frac{1}{L_j}\left[a(X_j-X_{j-1})+b(Y_j-Y_{j-1})\right](Y_j-Y_{j-1})$$

$$\frac{\partial L}{\partial d}=\sum_{j=2}^{m}\frac{1}{L_j}\left[d(X_j-X_{j-1})+e(Y_j-Y_{j-1})\right](X_j-X_{j-1})$$

$$\frac{\partial L}{\partial e}=\sum_{j=2}^{m}\frac{1}{L_j}\left[e(X_j-X_{j-1})+e(Y_j-Y_{j-1})\right](Y_j-Y_{j-1})$$